Tessellation of a stripe

Piotr Garstecki[1,2,*] and George M. Whitesides[1,†]
[1]*Department of Chemistry and Chemical Biology, Harvard University, 12 Oxford St., Cambridge, Massachusetts 02138, USA*
[2]*Institute of Physical Chemistry, Polish Academy of Sciences, Kasprzaka 44/52, 01-224 Warsaw, Poland*
(Received 31 August 2005; published 7 March 2006)

This paper describes enumeration of a class of topologically distinct periodic divisions of a stripe. Optimization of the geometry of these periodic tilings—optimization that yields minimum total perimeter of the tiles—gives a set of physically plausible periodic structures of monodisperse, two-dimensional foams bounded by two parallel walls. Evaluation of the minimum total perimeters of the lattices that we enumerated suggests two possible lower bounds for the mean perimeter of tiles forming periodic coverings of a stripe.

DOI: 10.1103/PhysRevE.73.031603 PACS number(s): 02.40.−k, 47.54.−r, 05.65.+b, 83.80.Iz

I. INTRODUCTION

We have described an experimental system that generates a family of periodic lattices of bubbles packed in microfluidic channels [1]. We wish to understand the mechanisms that form these lattices. A part of our study has investigated the possible topologies that can be achieved by tessellations of a stripe (a section of a plane bounded by two parallel lines). We also evaluate the "energies"—total perimeters of the edges of the tiles—of these tilings for a fixed topology and fixed ratio of the size of equal-area tiles to the width of the stripe. The results of this evaluation provide clues to the selection rules that guide the experimental system, and suggest two possible lower bounds for the mean perimeter of equal-area tiles forming periodic coverings of a stripe. These suggestions of lower limits of the perimeter of tiles covering a bounded plane provide a loose analogy of the "honeycomb conjecture," which suggests that hexagons tile the plane with the smallest perimeter. While the honeycomb conjecture has recently been proved formally [2], the questions about the topology and geometry of confined networks remain open for further numeric and analytical treatment.

Many important properties—i.e., mechanical, electronic, magnetic, or photonic—of materials depend both on chemical composition and on geometrical structure. These structures can sometimes be explained with the use of simple topological and geometrical principles. An example of a relation between simple optimization criterion and a structure that determines the physical properties is the honeycomb problem [and its three-dimensional (3D) equivalent], which can be stated as follows: "What is the division of a plane (3D space) into equal-area (equal volume) tiles that yields the lowest total length (surface area) of the boundaries between the tiles?" These problems are typically difficult. While the conjecture about tessellation of a plane has been proven [2], the three-dimensional problem is open: the solution conjectured by Lord Kelvin [3] has been improved by Weaire and Phelan in 1994 [4,5], but no analytical treatment is available to date.

Presence of boundaries and additional constraints complicate the solutions to the geometric and topological problems of division of space even further. For example, the simple problem of minimization of interfacial energy in a system composed of two immiscible phases has a global minimum corresponding to a macroscopic separation. Adding the requirement of a preferred (spontaneous) Gaussian curvature of the interface between the phases generates a variety of beautiful bi- and multi-continuous periodic structures [6–8]. In the world of foams, confinement of monodisperse bubbles to a capillary induces appearance of a range of intricate geometrical structures [9].

Topology of the network (or interconnectivities of the nodes forming the unit cell) can be a boundary condition for the optimization of its geometry. It is possible to enumerate whole classes of topologically distinct networks. Such enumerations provide important clues into the questions of possible arrangements of matter. For example, generation of a class of three dimensional networks [10] and geometrical optimization of the enumerated topologies lead to prediction of physically plausible structures of zeolites [11,12]. In principle, each of the topologically distinct tilings or networks can lead (when subject to the optimization of the geometry according to an appropriate energy functional) to a stable or metastable structure with distinct characteristics.

A convenient way to introduce boundary conditions and to guide self-organization is to introduce confinement. This approach often leads to novel structures that are either impossible, or difficult to observe in unbounded samples. For example, two-dimensional (2D) rhombic lattices of colloids can be obtained by the use of confinement of a microchannel [13]; small clusters of particles that minimize the second moment of the mass distribution were obtained by confining colloids to a shrinking droplet [14]; the use of the confinement of a microchannel has also been demonstrated to be an effective way to order the pattern of defects in a liquid crystalline sample [15]. Topological characteristics of both ordered [16–18] and disordered [19] patterns in microphase separation in amphiphilic mixtures also display a sensitive dependence to the size of the confined space.

The work described in this paper is motivated by an experimental observation of quasi two-dimensional periodic lattices of monodisperse bubbles in microchannels [1]. In this experiment the bubbles are ejected individually into a

*Email address: P.G. garst@ichf.edu.pl
†Email address: G.M.W. gwhitesides@gmwgroup.harvard.edu

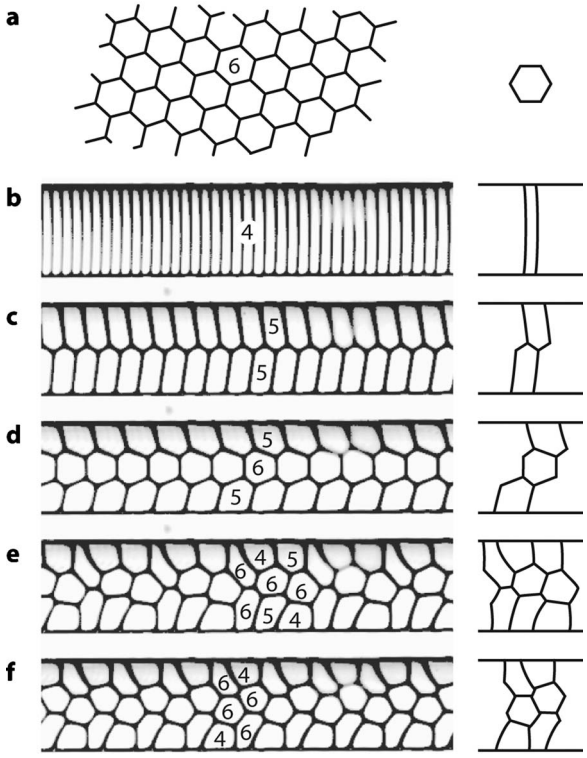

FIG. 1. (a) The honeycomb structure and its translational unit cell. (b) to (f) Experimentally observed structures of quasi-two-dimensional foam. The numbers indicate the number of neighbors (or of the sides) of each bubble in the translational unit cell. The unit cells are depicted on the right of each inset. The structures shown in insets (b) to (d) belong to the *hex-n* family: *hex-one*, *hex-two*, and *hex-three*, respectively. We called the structure shown in (f) *snake-skin* and the one shown in inset (e) *hybrid*. The details of the experiment are described in Ref. [1]. Here, we see the lattices in the "top" view (the line of view is orthogonal to the plane of the channel in which the lattices form.). The lateral size of the bubbles is much larger than their height; the bubbles do not wet the walls of the channel and are squeezed between bottom and top walls, separated from them by thin, wetting, film of the liquid. The bubbles form quasi-two-dimensional lattices; the two-dimensional geometry is only an approximation since the interfaces between bubbles are curved both in and out of the plane of the channel.

microfluidic channel characterized by a very large aspect ratio of its width to its height. The bubbles divide the space (or area of the floor of the channel) into patches of equal volume (or surface area). Although these lattices of bubbles minimize their interfacial energy locally, the system was often trapped in multiple local minima, and formed a variety of periodic structures [Figs. 1(b)–1(f)]. This behavior is in a vivid contrast to that of two-dimensional monodisperse foams in unbounded space, in which case the only structure observed, the honeycomb lattice, yields the global minimum of interfacial energy [Fig. 1(a)]. The observation of multiple stable structures of foams prompted us to pose three questions. (i) What periodic tessellations of a stripe (that is, a region of a plane bounded by two parallel lines) are possible? (ii) What are the relative interfacial energies (or equivalently, what are the total perimeters) of these lattices? (iii) Does the probability of formation of a lattice correlate

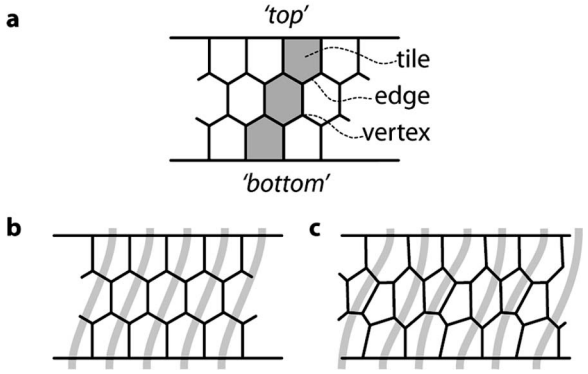

FIG. 2. (a) A schematic illustration of the terms that we use to describe the periodic tilings. The tiles forming the translational unit cell are highlighted with the gray color. In the text we refer to the top and bottom walls that confine the tiling to a stripe. (b) The *hex-three* lattice with one of possible choices of columns marked with thick gray lines. (c) An example of a periodic tiling that cannot be represented within the columnar model.

with its energy? The first question is interesting both fundamentally and for its possible applications in generating microstructures. The second and third questions address the selection rules for the appearance of these intriguing patterns.

We answer the first question partially by enumerating a set of topologically distinct periodic tessellations of a stripe. We explain the combinatorial model that we employed, and the bounding conditions that we used for the enumeration, together with its results, in Sec. II. In order to find the geometry of each lattice that yields the locally minimum perimeter of the patches, we used a numerical simulation; we outline this procedure in Sec. III. Section IV contains the results of simulations, and a comparison of those simulations with analytical calculations performed for the family of *hex-n* lattices. We supplement this section with results of a simulation in which we applied a pressure gradient along the stripe in order to verify whether it influenced the ranking of the total perimeters of the structures observed in experiment. We conclude the paper with a discussion of our results and with a postulate of possible lower bounds for the mean perimeter of tiles forming periodic coverings of stripes.

II. ENUMERATION OF A CLASS OF TOPOLOGICALLY DISTINCT TESSELLATIONS OF A STRIPE

Terminology. We start by defining the terms (Fig. 2) that we will use in the discussion that follows. The structures that we describe are two dimensional, and they are bounded by two parallel lines; we call these lines "walls." We refer to the area between the walls as a "stripe" but sometimes we also use the term "channel" to correspond to the microchannels used in our experiments. The terms "tile," "patch," and "bubble" all correspond to a surface bounded by a number of sides or edges. A side can either mark a boundary between two adjacent (neighboring) tiles, or it can coincide with a line segment belonging to one of the two walls. The sides (or edges) come together at nodes (or vertices). The tiles cover the area of the stripe completely, and the covering is peri-

odic: for each lattice, we can identify a translational unit cell that is composed of N individual tiles.

The fundamental characteristics of each of the lattices observed in our experiment [1] is its topology, the set of number of neighbors of each bubble in the unit cell. In order to find at least a partial answer to the question "what are the possible tilings of a stripe?" we need to enumerate topologically distinct periodic divisions. There is a number of methods for generating random [20,21] and periodic tilings of a plane [22–24]. Here, we employ a variation—one that takes into account the boundaries and periodicity of the tilings—of a method introduced by Fortes [21] for generation of "columnar" networks.

Columnar model. The translational unit cells of all of the structures that we observe in experiment can be represented as a union of "columns" [see example in Figs. 2(a) and 2(b)]. We use this model to enumerate a set of topologically distinct periodic tilings of a stripe. Importantly, not all periodic tilings can be represented in this way [Fig. 2(c)] and by using the columnar model we are restricting our results to only a class of periodic tilings. It is also important to note, that although it has been proven [25] that equilibrium structure of a 2D foam on an unbounded plane, formed by congruent bubbles must be periodic, it is not known if the energy minimizing structure of foam in confinement must be periodic or regular. Thus, limiting our results to periodic tilings that can be described within the columnar model, we cannot assess definitely the ground state of a confined two-dimensional foam.

Formally, we define a "column" as a union of tiles that stretches from one wall to the other with the following constraints: (i) if a tile within a column touches a wall, it can neighbor with at most one other bubble from the same column, (ii) all other bubbles within a column neighbor with exactly two other bubbles belonging to the same column. Finally, each tile belongs to only one column. We will only enumerate lattices which unit cells can be represented as a union of columns.

Enumeration. We enumerate the possible lattices by constructing the unit cells of a number C of columns, each (ith) column containing n_i bubbles. The topology of the lattice is determined by the positioning of the edges of the tiles. This positioning can, in turn, be enumerated within the construction that we describe below.

Each column is bounded from top and bottom by the walls, and from left and right by a union of a set of edges. This union of edges (or "side of the column") can in turn be represented as a line segment, spanning from the bottom to the top wall, with a number of nodes on it. Some of the nodes are formed by edges that lie to the left of the side of the column (and we refer to this nodes as "left nodes" and denoted them with the symbol "L") and some are made by the edges that lie to the right of the side of the column ("right" nodes, "R"). The structure of the side of a column can be represented by a sequence of left and right nodes. It is enough to consider only one side of the column: the right side of a given column is the same as the left side of the column that is adjacent to it from the right. The right side of the right-most column of the unit cell is the same as the left side of the leftmost column in the unit cell, following from the periodicity of the lattice.

All possible topologies of the periodic lattices that can be represented within the columnar model are determined by the sequences S_i of the left and right nodes on the sides of the columns. Figure 3 shows an example of an enumeration of possible sequences S_i for a unit cell comprising two columns ($C=2$) with three and two bubbles ($n_1=3$, $n_2=2$) in them. The right side of the first column [denoted with "S_1" in Fig. 3(a)] has three bubbles to the left (two left nodes) and two bubbles to the right (one right node) and there are three possible sequences of these nodes (RLL, LRL, and LLR). The right side of the second column [denoted with "S_2" in Fig. 3(a)] has two bubbles to the left (one left node) and, by the periodic boundary condition, three bubbles to the right (two right nodes); there are three possible sequences of these nodes (LRR, RLR, and RRL).

General expression for the number N_i of possible sequences S_i of nodes in ith column is $N_{i<C}=[n_i+n_{i+1}-2]!/[n_i-1]![n_{i+1}-1]!$, and $N_C=[n_C+n_1-2]!/[n_C-1]![n_1-1]!$. In the example shown in Fig. 3, $N_1=3$ and $N_2=3$. The total number of combinations (possible arrangements of the edges within the unit cell) is $P=\Pi_{i=1}^{C}N_i$. In our example, $P=9$, and all the combinations are shown in panels 3(b)–3(k).

For each combination of sequences of nodes, we calculate the number of neighbors (connectivities) m_{ij} of each (jth) bubble in each (ith) column, and encode these numbers in the form of C n_i vectors $V_i=[m_{i1},\cdots,m_{in_i}]$. The set of vectors V_i encodes the topology of the unit cell.

Elimination of redundant lattices. Some of the combinations of sequences S_i lead to the sets of connectivities V_i of the bubbles that are related to each other by some symmetry operation, and thus do not introduce distinct topologies of the tiling. In order to eliminate these redundancies, we take into account the following symmetries (and all their combinations): (i) identity: $I(m_{ij})=m_{ij}$, (ii) horizontal mirror symmetry $M_h(m_{ij})=m_{ik}$, with $k=n_i+1-j$, (iii) vertical mirror symmetry $M_v(m_{ij})=m_{kj}$, with $k=C+1-i$, and, (iv) translations $[T_k,\ k\in(1,C-1)]$ of the order of columns: $T_k(m_{ij})=m_{rj}$, where $r=i+k$ if $i+k\leqslant C$ and $r=i+k-C$ otherwise. Since we are taking into account unit cells comprising at most three columns the last symmetry operation can be denoted simply as all possible swapping of the first (column) indices in all the pairs of columns that contain the same number of bubbles: $p(m_{ij})=m_{kj}$, for all i and k for which $n_i=n_k$. In practice we enumerate all possible sets of connectivities V_i; for every new V_i we compare it (and all its images created by applying the symmetry operations M_h, M_v and T_k) with the listed set of topologically distinct lattices and if we do not find any match, we add the set to the list of enumerated lattices.

In the example illustrated in Fig. 3, the first set—called "$t12$"—[Fig. 3(b)] is new (and is enlisted as a distinct topology, we marked this fact on the figure by encircling the labels of the new, topologically distinct unit cells). The second unit cell—"$t13$"—[Fig. 3(c)] is also new and distinct, and so is the third [Fig. 3(d)]. The fourth set [Fig. 3(e)] is related to $t13$ by horizontal mirror symmetry (M_h) to the set shown in Fig. 3(c) and we eliminate it from the list.

Results of the enumeration. We have enumerated all pos-

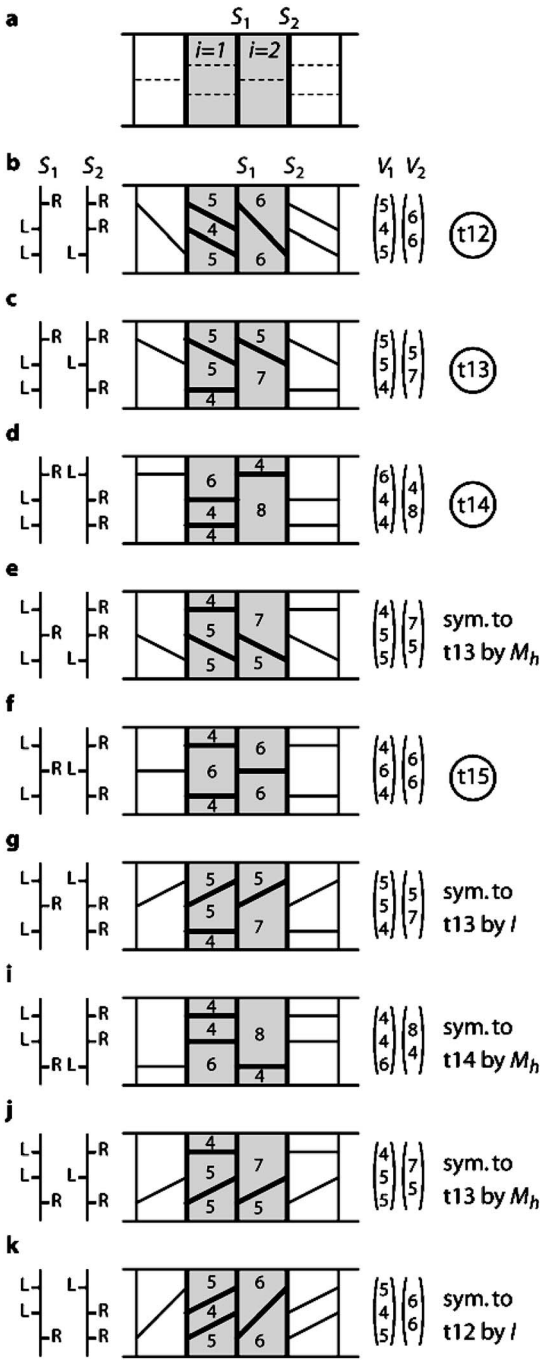

FIG. 3. A scheme exemplifying the enumeration procedure used. (a) The unit cell comprises two columns, with 2 and 3 tiles in them. Insets (b) through (k) show the nine possible combinations of the sequences S_1 and S_2 of the left (L) and right (R) nodes. The resulting arrangements of tiles, with the tiles comprising the unit cell highlighted with gray color, and with the number of neighbors of each tile, are shown in the center of each inset. On the right of each panel we show the corresponding vectors V_1 and V_2. The first three combinations [insets (b) through (d)] and the fifth one (f) are new and are put on the list of the topologically distinct tessellations of a stripe as lattices labeled $t12$, $t13$, $t14$, and $t15$, respectively. All the other combinations are redundant: they can be mapped onto the listed lattices by one of (or a combination of) the symmetry operations: identity (I), horizontal or vertical mirror symmetry (M_h or M_v, respectively), and translations of the columns (T_k).

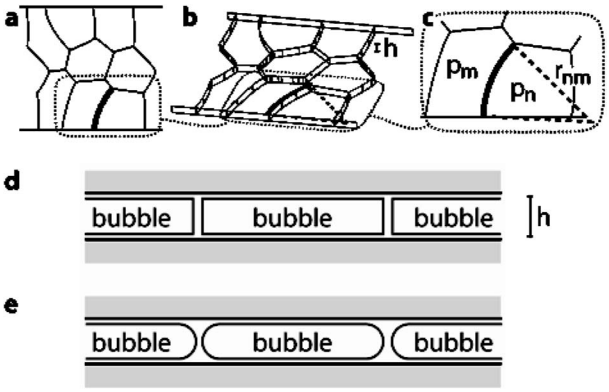

FIG. 4. A two-dimensional tessellation of a stripe (a) is equivalent to a planar cross section of an idealized model of a quasi-two-dimensional foam confined to a channel of uniform width and height (b). We calculate the planar curvature of a bubble-bubble interface (an exemplary interface is highlighted with thick solid line in all insets) by assigning pressures p_n to all the bubbles and calculating their difference $(p_n - p_m) = \gamma / r$, where γ is the value of interfacial tension and r is the radius of curvature [highlighted with dashed line in inset (c)]. The assumption of a two-dimensional geometry of the bubble-bubble interfaces is only an approximation; in reality the interfaces between bubbles do not look as we pictured them in inset b or d, but are also curved in the planes that are orthogonal to the plane of the channel [illustrated in inset e]. In our calculations we neglect this curvature ($\kappa \sim 2/h$) because it remains approximately constant regardless of the geometry of the bubbles in the plane of the channels, provided that $r_{nm} > h/2$.

sible tilings within the following constraints: (i) the number of columns is less than or equal to three, and (ii) the number of bubbles in the column is less than or equal to three, with the condition that $n_i \geq n_j$ if $i < j$. With these constraints, we obtained 371 combinations of sequences S_i, which yielded 69 topologically distinct periodic lattices.

III. OPTIMIZATION OF THE GEOMETRY—FINDING MINIMUM PERIMETERS

We are interested in the "energies" of each of the topologically distinct arrangements of tiles. The energies of the two-dimensional tilings are proportional to the total perimeters of the tiles. The geometry of the lattices is subject to two boundary conditions. One is the fixed topology of the lattice, and second is the ratio of the size of (surface area) of the tile to the width of the stripe. Respecting these boundary conditions, we found the geometries that minimize the total perimeter using a computer simulation that borrows from the dynamics of two-dimensional foams [26–28].

In this analogy, each tile corresponds to a quasi-two-dimensional bubble [Figs. 4(a) and 4(b)] which has a uniform height h and a cross section in the plane of the channel which coincides with the shape of its corresponding tile. We parametrize the size of the tiles by their surface areas A_i. In each simulation we constrain this areas to a value A_0; A_0 is related to the length of the side a_0 of a perfect hexagon of the same area $a_0 = 3^{-3/4} 2 A_0^{1/2}$.

Evolution of curvatures and pressures. In two dimensions

the equivalent of the interfacial energy of a lattice is the sum of the perimeters l of the tiles—that is the total length of the sidewalls of all the patches into which the surface area of the stripe is divided. In order to asses the shape (curvature) of the interfaces between the tiles, we associate with each tile a pressure p_n and we calculate the radius of the planar curvature of these interfaces as $r_{nm}=\gamma/\Delta p$, where $\Delta p=p_n-p_m$ is the difference of "thermodynamic" pressures inside the nth and mth tile. Fixing the surface areas of the tiles ($A_n=A_0$) is equivalent to an approximation that the pressure $p_L=\gamma/r$ associated with the planar curvature of the interfaces between the tiles is negligibly small in comparison to the thermodynamic pressures p_n. This approximation corresponds well to our experiments [1]: if we take volume of the bubble $V_0=hA_0=cp^{-1}$, where c is a constant ($c=nRT$ for an ideal gas), then the change in the surface area of the bubble introduced by the Laplace pressure p_L is $A_0-A=cp_L/p(p+p_L)$, and $(A_0-A)/A_0=p_L/(p+p_L)$. In our experiments, the thermodynamic pressure is on the order of $p\approx 10^5$ Pa, while the typical Laplace pressure is $p_L\approx 10^2$ Pa (for $\gamma\approx 3\times 10^{-2}$ N/m, and $r\approx 300$ μm), yielding $(A_0-A)/A_0\approx 10^{-3}$.

Limitation of the two-dimensional model in description of the quasi-two-dimensional foams. The two-dimensional model that we employ establishes the total perimeters of strictly two-dimensional tilings. We do relate these total perimeters to the interfacial energies of the quasi-two-dimensional lattices observed in our experiments [1] but we note, that the perimeters of the two-dimensional lattices provide only an approximation of the component of the interfacial energies of the real lattices. The two-dimensional model cannot assess the stability of the real, quasi-two-dimensional lattices in which at least one of the edges of any of the bubbles has a length (in the plane of the channel) which is shorter than, or similar to, the height of the channel. The reason for this limited relevance is that (by definition) the two-dimensional model does not take into account the curvature of the bubble interfaces that is not confined to the plane of the channel. In reality the interfaces between the bubbles and the liquid are curved in the plane of the cross section of the channel [Fig. 4(d)]. This curvature can be approximated to be on the order of $\kappa_{cross}\approx 2/h$ and to be constant regardless of the shape of the bubble in the plane of the channel, provided that the curvature κ_{plane} in the plane of the channel of any given interface between the nth and mth bubble given by $\kappa_{plane}\approx 1/r_{nm}$ is comparable to, or smaller than κ_{cross}. We expect that when $\kappa_{plane}\approx\kappa_{cross}$ or $\kappa_{plane}>\kappa_{cross}$ the real (three dimensional) geometry of the interfaces can affect the stability of the shapes that we evaluate numerically within the two-dimensional model, and this model no longer will provide a reasonable approximation of the structure of the quasi-two-dimensional foam.

Minimization of the total perimeter within the two-dimensional model. The evolution of the structure of the lattice in the simulation proceeds in the following steps. We first calculate the line-tension forces acting on each vertex: each edge pulls the vertex with a force of absolute value $|F|=\gamma h=\sigma$, where σ corresponds to the effective line tension of an edge in the 2D model, and a direction coinciding with the tangential direction of the edge and pointed away from the vertex [Fig. 5(a)]. In our model, we assume that the surface tension is constant: that is, we assume that the interfaces are well saturated with surfactant and there are no dynamic surface tension effects. Practically, in our numerical procedure, we kept $|F|\equiv 1$. We then calculate a dimensionless net force $F^*=(\Sigma F)/\gamma h$ acting on any given vertex, and we move this vertex by a displacement $d=F^*\xi w$, where ξ is a dimensionless constant that determines the rate of motion of the vertex (we typically used $\xi=10^{-2}$ in the beginning of the optimization procedure and smaller values (down to $\xi=10^{-5}$) at the end of minimization of the perimeter). We employ the additional condition that the vertices lying on the walls of the channel stay on these walls: that is, for these vertices we take the component of F^* in the direction of the walls and move the vertex along the wall. After moving the vertices we iteratively adjust the pressures in all the bubbles and the curvatures of the bubble-bubble interfaces until the surface areas of all the bubbles are equal to the target surface area. Relocation of the vertices and the adjustment of pressures are both subject to the periodic boundary conditions: the rightmost vertices of the unit cell are moved in synchrony with the leftmost ones, and the curvature of the bubble-bubble interfaces at the boundaries of the unit cell are calculated using periodic boundary conditions for the pressures inside the bubbles. Once vertices are moved and pressures adjusted, we repeat the steps outlined above until the structure reaches a stationary state in which all of the forces acting on the edges inside the channel are exactly balanced, and the net force acting on the vertices located on the walls of the channel is perpendicular to the direction of the wall. If the given topology of the lattice, combined with the prescribed surface area A_0 of the tiles leads to a physically plausible structure, the geometry of the bubble-bubble interfaces automatically satisfies the Plateau rule: edges meeting at vertices inside the channel make angles of 120° [Fig. 5(a)]. Some topologies, however, do not have a physically plausible ground state. In such a case, in the course of the optimization of the geometry at least two of three-coordinated vertices come together. In an experiment this fusion would lead to a topological transformation ($T1$) of switching the neighbors [29] and the topology of the lattice would change. Since we are interested in the ground states of a list of enumerated (and fixed) topologies of the periodic lattices, we do not allow topological transformations and the two vertices stay together [Fig. 5(c)]. We deem such structures not physically plausible, and we remove them from the list of possible structures of foam for a given A_0.

During the evolution, we monitor the total length of the perimeter l of all N bubbles comprising the translational unit cell of the lattice. We normalize this total perimeter by the perimeter of the perfect tiling of a plane, that is, by the perimeter of N regular hexagons: $l^*=l/N(6a_0)$. This normalization allows us to determine how much the tessellations of a stripe deviate from the optimal solution for an infinite plane, the honeycomb lattice. Figure 5(d) shows that l^* decays monotonically during the optimization procedure until it reaches a minimum value for the given a_0 and topology of the lattice. We note that due to the construction of the numerical procedure we used to optimize the geometry (constant force exerted on the edges by each vertex, and varied time step), we do not expect to recover the dynamics of an

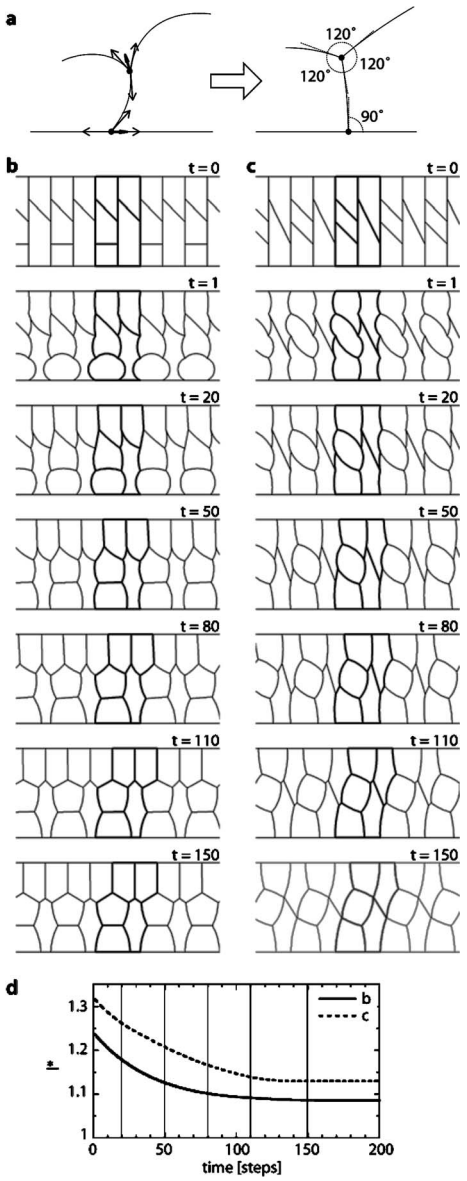

FIG. 5. (a) A schematic illustration of the simulation scheme for optimization of the total perimeter of the tiles. We calculate the forces F (thin, long arrows) exerted by the edges of the tiles on the vertices. We use the net, nondimensional forces F^* (the thick, short arrow exemplifies the direction of F^*) to move the vertex by a distance $d=F^*\xi w$, where ξ is a constant that determines the rate of evolution. We employ the condition that vertices located on the side walls can move only along the walls. The evolution stops when the angles between the films (edges) connected to all the vertices located inside the stripe are 120°, and the films connected to the vertices located on the walls make right angles with them. (b) and (c) An example of an evolution of two structures from the geometry of the columnar model to the states of lowest energy (total perimeter) allowed by their topology. Structure in inset (b) leads to a physically plausible ground state, while the structure shown in (c) leads to a structure with two paired vertices and has to be excluded from the list of plausible topologies of two-dimensional foam. We indicate the number of simulation steps corresponding to each image in the insets ($\xi=10^{-2}$). Inset (d) shows the change of the total perimeter of the structures shown in (b) and (c) with the number of simulation steps.

actual quasi-two-dimensional foam, and the time scale shown in Fig. 5(d) is not linearly related to the physical time. It is only the final, equilibrium, geometry of the structure that we expect to correspond to the geometry of two-dimensional foam that minimizes the total perimeter of the tiles.

A question also arises whether the perimeter-minimizing geometry that we find numerically for given topology of the lattice and surface area of the tiles represents a unique solution of the problem. In other words: is it possible that, for any given topology and surface area of the tiles, that there is more than one geometry of the lattice that represents a local minimum of the total perimeter? To the best of our knowledge there is no formal proof that the 2D equal-area foams have a unique perimeter-minimizing solution. A proof of uniqueness of the energy-minimizing state for a similar system of string networks can, however, be found in recent work by Delaney *et al.* [30]. Our intuition tells us that the geometries output by our routines do represent unique solutions to the problem of minimizing the perimeter. We can support this postulate only indirectly: we varied the initial conditions for several topologies and sizes of the tiles in our simulations, and we observed that the final, perimeter-minimizing, geometry does not depend on the starting configuration.

IV. RESULTS

Family of hex-n tilings. Before we review of the results of our numerical procedures, we first consider the family of *hex-n* lattices [Figs. 1(b)–1(d)] that can be treated analytically. Figure 6 shows a schematic illustration of the geometry of a *hex-n* lattice, where n signifies the number of rows (of tiles) parallel to the walls of the channel. We call these lattices *hex-n* because all the tiles that are not adjacent to the walls retain the topology of the honeycomb lattice, and each bubble has six neighbors. As outlined in Fig. 6, we can calculate the characteristic dimensions of the *hex-n* tiling taking advantage of the following constraints: (i) the surface area of the translational unit cell is equal to nA_0, and hence $z=nA_0/w$, (ii) the width of the channel is $w=n(y+x)$, and (iii) the angle between the edges inside the channel is 120° (so $z=2\sqrt{3}x$). The two last conditions lead to $x=nA_0/(2\sqrt{3}w)$ and $y=(w/n)-nA_0/(2\sqrt{3}w)$. The sum of the lengths of all the edges in all bubbles (tiles) comprising the unit cell is $l=2(x+ny+z)+4(n-1)(x^2+z^2/4)^{1/2}$ Dividing by $n6a_0$ and simplifying we obtain Eq. (1), where $a^*=a_0/w$

$$l^*(n,a^*)=a^*[(3/4)(n-1)+\sqrt{3}/2]+a^{*-1}[3n]^{-1}. \quad (1)$$

Figure 6(b) shows a family of curves $l^*_{hex\text{-}n}(n,a^*)$ for $n=1$ to 7. Each curve $l^*(n,a^*)$ has a minimum $l^*_{min}(n)=[(n-1)/n+2/(\sqrt{3}n)]^{1/2}$ at $a^*_{min}(n)=[9n(n-1)/4+3\sqrt{3}n/2]^{-1/2}$. Interestingly, the whole family of curves is bounded from below by a linear function

$$l^*_{bound}=1+a^*(2\sqrt{3}-3)/4. \quad (2)$$

We calculated the linear coefficient $(2\sqrt{3}-3)/4$ by observing that for every n there is a value of $a^*=b(n)$ for which Eq. (3) holds

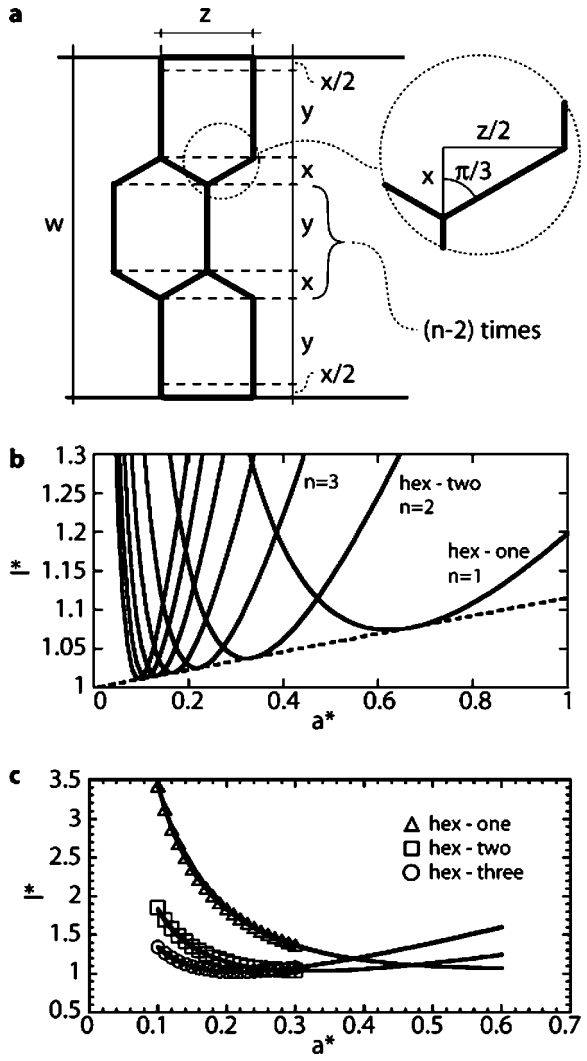

FIG. 6. (a) An illustration of the geometry of the *hex-n* family lattices (*hex-three* shown). We use the symbols defined in the figure for the derivation of the perimeter of these lattices. (b) A plot of the non-dimensional (normalized by the perimeter of n hexagonal cells) mean perimeter of the tiles in the *hex-n* family lattices (*hex-one* through *hex-seven*): $l^*=l/6na_0$, plotted as a function of the nondimensional ratio of the size of the tile to the width of the stripe: $a^*=a_0/w$. The minimum mean perimeter of the *hex-n* family lattices is bounded from below by a function l^*_{bound} shown with the dashed line in the figure. (c) Comparison of the analytically and numerically evaluated perimeters of the *hex-one* through *hex-three* lattices.

$$l^*(n,b) = 1 + dl^*/\,da^*|_b b \tag{3}$$

with $b(n)=2/(3n)$, and $dl^*/da^*|_b=(2\sqrt{3}-3)/4$ independent of n.

Verification of the accuracy of the simulation. The above calculations offer a convenient check of the accuracy of the perimeters established with our numerical simulations. We compared [Fig. 6(c)] the numerical results for *hex-one*, *hex-two*, and *hex-three* lattices for $a^* \in (0.1, 0.3)$; the largest absolute value of a difference $(l^*_{analytical}-l^*_{numeric})$ was 3.4×10^{-5}. In view of this comparison, we present all the

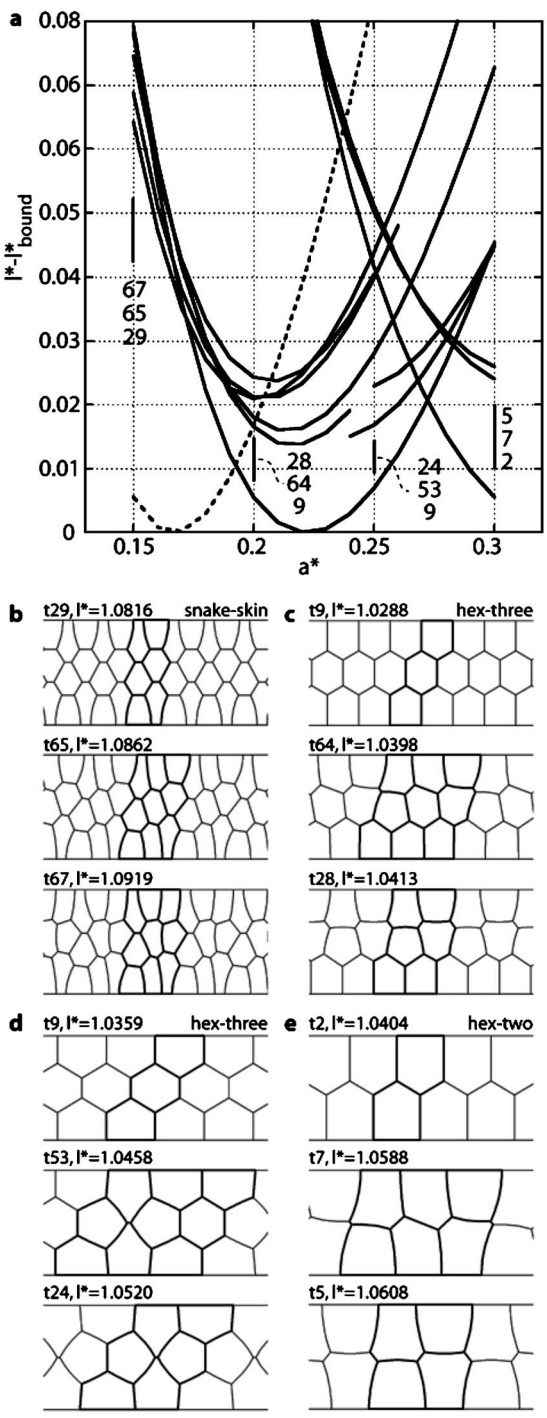

FIG. 7. (a) The numerically evaluated normalized perimeters l^* (less the lower bound of the perimeter l^*_{bound}) for a set of enumerated lattices. The criterion for a given unit cell to be entered into the set was that the lattice has to be among the three lattices that yield three lowest values of l^* for any value of a^* that we examined $a^* \in (0.15, 0.3)$. The numbers indicate the numbers of the topologies that yield the lowest values of l^* for $a^*=0.15$, 0.2, 0.25, and 0.3. The dashed line gives analytically calculated values of l^* for the *hex-four* lattice. Insets (b) through (e) show the geometries of the triplets of lattices that yield the lowest values of perimeters within the enumerated set. Above each picture we give the number of the lattice in the enumerated set ($t29$, $t65$, etc) and the lowest value of l^* for given topology and value of a^*.

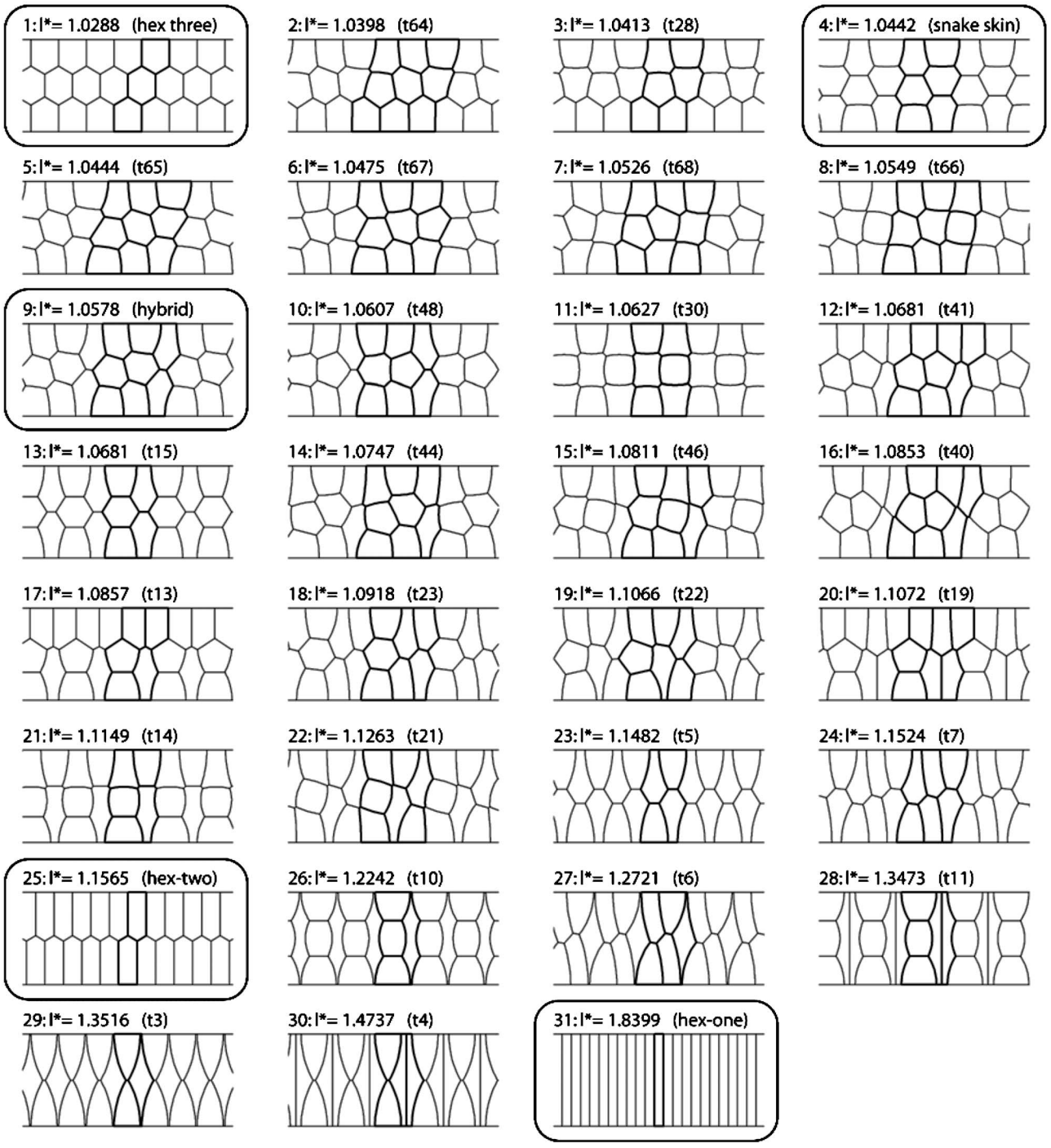

FIG. 8. The 31 (out of 69 enumerated) lattices that yield physically plausible minima of their perimeters for $a^*=0.2$. The structures are displayed in order of increasing perimeter l^* from left to right and top to bottom. The inscription by each structure gives the ranking (with 1 corresponding to the lowest perimeter), the perimeter, and the name (number) of the topology. The lattices marked with rounded rectangles correspond to the structures observed in our experiment (see also Fig. 1).

perimeters (l^*) that we obtained numerically with four decimal digits.

"*Optimal tilings*." We have evaluated the ground states of each of the 69 enumerated tessellations for $a^* \in (0.15, 0.3)$ with a resolution of $\Delta a^*=0.01$. For each value of a^* that we examined, a different number of topologies yield physically plausible structures. For example, for $a^*=0.15$ we found 28 plausible geometries; for $a^*=0.2, 31$ tessellations yielded physically plausible structures of two dimensional foam; for $a^*=0.25$ and 0.3, the number of physically plausible structures was 39 and 42, respectively.

For each value of a^*, we can rank the plausible structures in order of increasing mean perimeter of the tiles that make them. The type of the structure that yields the lowest perimeter depends on the value of a^*. Figure 7(a) shows the evolution of the perimeter $l^*(a^*)$ (plotted as l^*-l^*_{bound}), for 11

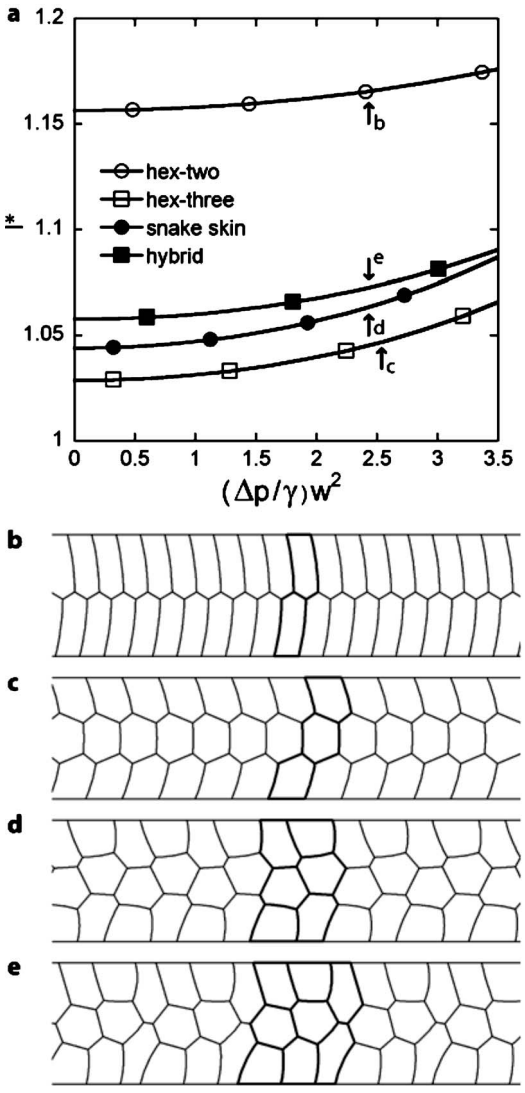

FIG. 9. The influence of the pressure gradient along the channel on the perimeter l^* and the geometry of the periodic lattices. Within the values of the pressure gradient that we tested in our simulations, the pressure gradient does not change the ranking of the lattices in terms of the length of their perimeters. The geometries of the lattices subject to a pressure gradient are similar to those observed in experiment (see Fig. 1).

lattices. The criterion for choosing these lattices was that each one of them was one of the three lattices yielding three lowest values of perimeter for at least one of the values of a^* that we examined. For example, for $a^*=0.15$, the *snake-skin* lattices yields the lowest perimeter; the second and third lowest values correspond to the lattices that we called $t65$ and $t67$ [Fig. 7(b)]. In Figs. 7(c)–7(e) we show analogous triplets for $a^*=0.2$, 0.25, and 0.3 in Fig. 7.

We emphasize that these are not necessarily the lowest possible energies for given value of a^*, as we have enumerated only a finite set of periodic tilings of a stripe. For example, for $a^*=0.15$, the lattice *hex-four*, for which we know the perimeter l^* analytically, provides a better solution than any of the structures that we enumerated numerically. For this value of a^*, it is plausible that other arrangements with four bubbles in a column might yield lower values of the total perimeters than the ones we considered here. For small values of a^* (for example $a^*=0.15$) the lattices with only three tiles in a column have bubbles (tiles) elongated in the direction perpendicular to the direction of the walls of the channel, and thus diverging significantly from the ideal hexagonal shape. Similarly, we can expect that for $a^*=0.2$, the higher order lattices might change the ranking of lowest perimeters that we recorded in our simulations. For higher values of a^*, as for example for $a^*=0.3$, it is likely that our set of lattices includes the ones that yield the lowest perimeters.

Comparison with the experiment. In Fig. 8 we show all of the 31 optimized lattices that yield physically plausible minima of energy for $a^*=0.2$, which is approximately the value for which we recorded the experimental images presented in Fig. 1. Although, as we discussed above, this ranking of lattices in terms of their perimeter is most likely *not* complete (because we considered only lattices with a maximum of three bubbles in a column) we can establish that there are possible arrangements of bubbles that yield lower values of the total perimeter than the lattices observed experimentally. Only the *hex-three* lattice, which we observe in experiment, coincides with the lowest possible energy. The *snake-skin* lattice ranked fourth, with two other lattices ($t64$ and $t28$) having lower energy; we have not observed them experimentally. The *hybrid* lattice ranked 9th, the *hex-two* 15th, and *hex-one* ranked 31st with the *highest* interfacial energy within the enumerated set. We emphasize that some of the lattices shown in Fig. 8 contain edges that are relatively short. For these lattices, the approximation of a two-dimensional geometry of the interfaces, is legitimate only if $l_{nm}>h/2$, where l_{nm} is the length of the interface between nth and mth bubble, and h is the height of the channel. Thus, in order to observe these lattices experimentally one should use a channel with a very large aspect ratio of the width to the height. In our experiments this aspect ratio was approximately $w/h\sim 30$, and the lattices containing edges with $l_{nm}<w/30$, would be unstable do to the truly three-dimensional character of these edges.

Pressure gradient along the channel. We also tested the influence of a pressure gradient ∇p along the channel on the ranking of energies (perimeters) of the lattices that we observed in our experiments. Technically, we first optimized the geometry of the interesting lattices in the absence of the gradient of pressure ($\nabla p=0$), and once we had obtained the state that minimized the perimeter, we fixed (immobilized) the vertices that lied on the walls of the channel and slowly increased the pressure gradient, allowing the structure to equilibrate to it. Technically, the only difference introduced into the numerical procedures, in order to account for the pressure gradient, is that when calculating the curvature of the bubble-bubble interfaces that coincide with the left and right boundaries of the unit cell, we supplemented the difference of pressures p_n-p_m, with an additional term $\Delta p=\nabla p\,(nA_0/w)$, where (nA_0/w) is the length of the unit cell comprising n bubbles. We parametrized the gradient of pressure by its nondimensional value $\nabla p^*=(\nabla p/\gamma)w^2$ and performed simulations for $\nabla p^*\in(0,3.5)$ as within this range the lattices deform to structures similar to those observed in experiment. Figure 9 illustrates both the evolution of the perimeter

$l^*(\nabla p^*)$ of four of the observed lattices and the simulated structures for $\nabla p^* \sim 2.5$. We found that the pressure gradient does not change the ranking of energies of the observed lattices and therefore cannot account for the change of probabilities of formation of them with the change of the rates of flow of the fluids through the system [1].

V. DISCUSSION

Minimum mean perimeter in equal-area tessellations of a stripe. Having evaluated the minimum perimeters of all the enumerated lattices we found no instance of the best (most energetically favorable) solution not belonging to the family of *hex-n* lattices. On the basis of this observation we put forward (although cannot prove) the following two postulates. The first, weaker, statement is that the function $l^*_{bound}=1+a^*(2\sqrt{3}-3)/4$ [Eq. (2)] forms the lower bound for the minimum mean perimeter of equal area tiles in a periodic tessellation of a stripe. The second, stronger, postulate is that there is no periodic, equal area, tessellation of a stripe that would yield a smaller perimeter than the perimeter of one of the *hex-n* lattices [Eq. (1)].

It would be interesting if either of these two postulates could be proven analytically; as the honeycomb conjecture [2] for an equal-area tessellation of an infinite plane.

VI. CONCLUSIONS

We have enumerated the topologies and optimized the geometry of a set of periodic tilings of a stripe. We find that the introduction of confinement generates a large number of periodic structures that correspond to local minima in interfacial energy. Some of these structures can be observed experimentally. Our numerical results suggest potential bounds for the lowest value of the perimeter of two-dimensional tilings of stripes.

Enumeration of topologies of two- and three-dimensional networks subject to confinement might lead to insights in areas remote from the physics of foams. For example, nanotubes offer strong confinement, and it has already been shown that it is possible to dope the space inside the tubes with atoms. It might be therefore interesting to ask what chemical networks are possible in strongly confined geometries.

Finally, we believe that the aesthetic appeal of the tiling patterns established through our numerical procedures prompts for the use of these tilings in the decoration of sidewalks, tracks and corridors.

ACKNOWLEDGMENT

P.G. acknowledges support from the Foundation for Polish Science. This work was supported by the U.S. Department of Energy under award DE-FG02-OOER45852.

[1] P. Garstecki and G. M. Whitesides (unpublished).
[2] T. C. Hales, Discrete Comput. Geom. **25**, 1 (2001).
[3] W. Thomson (Lord Kelvin), Philos. Mag. **24**, 503 (1887).
[4] D. Weaire and P. Phelan, Nature (London) **367**, 123 (1994).
[5] D. Weaire and R. Phelan, Philos. Mag. Lett. **69**, 107 (1994).
[6] V. Luzzati and P. A. Spegt, Nature (London) **215**, 701 (1967).
[7] W. T. Gozdz and R. Holyst, Phys. Rev. E **54**, 5012 (1996).
[8] R. D. Kamien, Rev. Mod. Phys. **74**, 953 (2002).
[9] S. Hutzler *et al.*, Philos. Mag. Lett. **82**, 297 (2002).
[10] O. D. Friedrichs *et al.*, Nature (London) **400**, 644 (1999).
[11] M. D. Foster *et al.*, Nat. Mater. **3**, 234 (2004).
[12] M. D. Foster *et al.*, Angew. Chem., Int. Ed. **42**, 3896 (2003).
[13] E. Kumacheva, P. Garstecki, H. K. Wu, and G. W. Whitesides, Phys. Rev. Lett. **91**, 128301 (2003).
[14] V. N. Manoharan, M. T. Elsesser, and D. J. Pine, Science **301**, 483 (2003).
[15] M. C. Choi *et al.*, Proc. Natl. Acad. Sci. U.S.A. **1001**, 17340 (2004).
[16] V. Babin and A. Ciach, J. Chem. Phys. **119**, 6217 (2004).
[17] A. Ciach, V. Babin, and M. Tasinkevych, Colloids Surf., A **208**, 51 (2002).
[18] J. Y. Cheng *et al.*, Adv. Mater. (Weinheim, Ger.) **15**, 1599 (2003).
[19] M. Gameiro, K. Mischaikow, and T. Wanner, Acta Mater. **53**, 693 (2005).
[20] G. Lecaer, J. Phys. A **24**, 1307 (1991).
[21] M. A. Fortes, J. Phys. A **28**, 1055 (1995).
[22] M. S. Delaney, MATCH **9**, 73 (1980).
[23] A. W. M. Dress, D. H. Huson, and E. Molnar, Appl. Comput. Electromagn. Soc. J. **49**, 806 (1993).
[24] O. Delgado-Friedrichs, Theor. Comput. Sci. **303**, 431 (2003).
[25] D. Weaire *et al.*, Proc. R. Soc. London, Ser. A **460**, 569 (2004).
[26] J. P. Kermode and D. Weaire, Comput. Phys. Commun. **60**, 75 (1990).
[27] N. Kern, D. Weaire, A. Martin S. Hutzler, and S. J. Cox, Phys. Rev. E **70**, 041411 (2004).
[28] S. J. Cox, Colloids Surf., A **263**, 81 (2005).
[29] D. Weaire and S. Hutzler, *Physics of Foam* (Oxford University Press, Oxford, 1999).
[30] G. Delaney, D. Weaire, and S. Hutzler, Europhys. Lett. **72**, 990 (2005).